

Effect of calcium on dissolution and precipitation reactions of amorphous silica at high alkalinity



Hamed Maraghechi ^{a,*}, Farshad Rajabipour ^b, Carlo G. Pantano ^c, William D. Burgos ^b

^a Laboratory of Construction Materials, Institute of Materials, Ecole Polytechnique Fédérale de Lausanne (EPFL), Switzerland

^b Department of Civil and Environmental Engineering, Pennsylvania State University, University Park, PA 16802, USA

^c Department of Materials Science and Engineering, Pennsylvania State University, University Park, PA 16802, USA

ARTICLE INFO

Article history:

Received 13 August 2015

Accepted 17 May 2016

Available online xxxx

Keywords:

Kinetics (A)

pH (A)

Glass (B)

Alkali-aggregate reaction (C)

Pozzolan (D)

ABSTRACT

A better understanding of silica dissolution–precipitation reactions at high pH aqueous solutions allows for promotion of favorable (e.g., pozzolanic) reactions and mitigation of deleterious (e.g., alkali-silica) reactions in concrete. In this paper, the kinetics and products of silica glass dissolution are studied as a function of solution pH, temperature, and availability of calcium. It was observed that dissolution rate versus time increases linearly with pH and reaches a maximum at pH = 14, with slower dissolution at higher alkalinities. In solutions with similarly high pH, but saturated with portlandite, glass dissolution is significantly slower. This is due to formation of a dense, low porosity, and strongly bonded C–S–H layer on the surface of glass, which serves as a barrier against diffusion of OH[−] and alkali ions towards the substrate glass. This protective layer forms only when Ca is abundant and portlandite saturation can be maintained on a local scale.

© 2016 Elsevier Ltd. All rights reserved.

1. Introduction

Several important chemical reactions in concrete, such as the pozzolanic, geopolymeric, and alkali-silica reactions (ASR) begin with dissolution of amorphous or otherwise metastable metal-silicate phases (e.g., from fly ash, slag, or reactive aggregates) into the alkaline pore solution of concrete. The dissolved species subsequently react and precipitate as a binding material, such as calcium silicate hydrate (C–S–H or C–(A)–S–H), or a swelling gel (e.g., ASR gel). Therefore, study of the dissolution and precipitation characteristics of metal-silicates in alkaline solutions helps in better understanding and controlling these reactions. For this purpose, commercial soda-lime and fused silica glasses were used as simple models in this study. A further goal of this research was to investigate the reactivity of soda-lime glass (a potential pozzolan or aggregate source obtained by recycling glass bottles and window plates [1]) in environments similar to concrete pore solution. The findings can also benefit the durability, in exposure to alkaline environments, of multi-oxide glasses encapsulating radioactive waste [2].

Specifically, the following objectives were pursued in this study:

1. To quantify the kinetics of silicate glass dissolution at high alkalinity (12.0 < pH < 14.9), similar to those that exist in the pore solutions of portland cement and alkali-activated concretes.

2. To investigate the nature and characteristics of solid products, resulting from dissolution of soda-lime glass.
3. To assess the effect of soluble calcium on (1) and (2). This is important as soluble calcium (e.g., portlandite) is abundant in portland cement concrete, and can affect the dissolution and precipitation of silica and formation/swelling of ASR gel [3–5].

In the following, a background on silicate glass interactions with aqueous solutions is presented. Next, a brief review on the use of soda-lime glass in concrete is provided, followed by description of the experiments in this study.

2. Interactions of silicate glass with aqueous solutions

Silicate glasses are composed of silica tetrahedral units (Fig. 1-a), connected to each other by bridging oxygens (BO), or to other atoms such as Na, K, Ca, or H through non-bridging oxygens (NBO) [6] (Fig. 1-b). The number of tetrahedral units containing 0, 1, 2, 3, and 4 bridging oxygens (Q⁰ to Q⁴) can be quantified using NMR spectroscopy [7,8]. Two main types of interactions between silicate glasses and aqueous solutions, namely leaching of alkalis and network (congruent) dissolution, are introduced in the following sections.

2.1. Leaching (ion exchange)

Leaching or extraction of alkali cations from glass occurs through diffusion of H⁺ or H₃O⁺ from the solution into the glass, to replace

* Corresponding author.

E-mail addresses: hamed.maraghechi@epfl.ch (H. Maraghechi), farshad@psu.edu (F. Rajabipour), cgp1@psu.edu (C.G. Pantano), wdb3@psu.edu (W.D. Burgos).

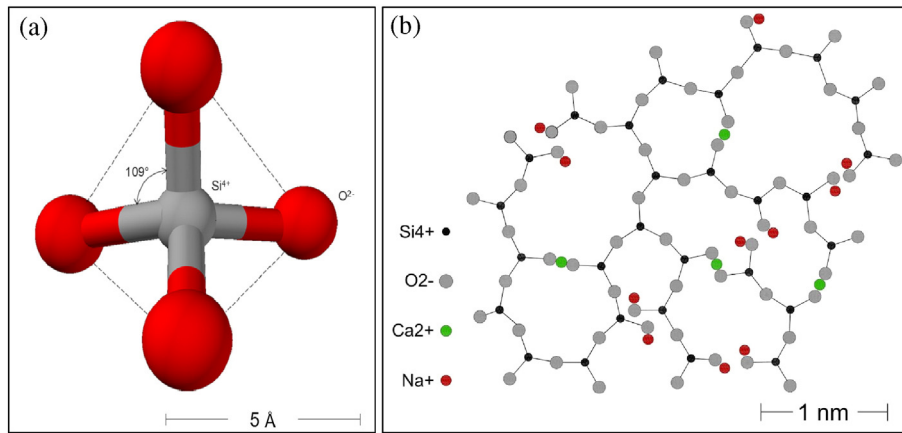


Fig. 1. (a) A silica tetrahedron where a silicon atom is surrounded by four oxygen atoms, (b) Two-dimensional representation of the atomic structure of soda-lime silica glass; bridging oxygens (BO) connect two Si atoms while non-bridging oxygens (NBO) are connected to one Si atom and one Ca or Na atom.

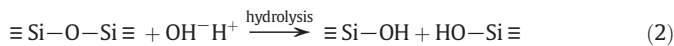
alkalis (e.g., Na^+) as seen in Eq. (1) [9]. Leaching becomes significant at lower (acidic) pH, and increases the pH of the solution [9–11].



Many aspects of alkali leaching from silicate glasses have been studied [12–14], including the papers by Scholze [15,16] and Bunker [8], which reviewed the mechanisms of water–glass interactions during leaching of cations. As alkalis diffuse out of the glass surface, a Si-rich altered layer, known as the gel-layer, forms which could condense and act as a barrier against further diffusion of ions into and out of glass [17]. As discussed below, the altered gel layer on the surface of glass can also form in exposure to alkaline solutions, and this has been documented within the domain of nuclear glass research [18].

2.2. Network (congruent) dissolution

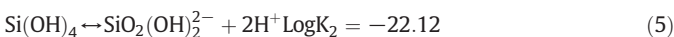
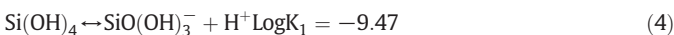
Network dissolution (or hydrolysis) occurs at high pH, where the polar siloxane ($\text{Si}-\text{O}$) bonds are broken through a nucleophilic attack of hydroxyl ions (OH^-), according to Eq. (2) [17,18]. In fact, the surface of silicate glass that is exposed to water is almost always hydrolyzed, and $\equiv \text{Si}-\text{OH}$ groups are abundant [19,20]. The reverse reaction in Eq. (2) is called “condensation”, as it results in liberation of water.



The forward reaction presented in Eq. (2) can proceed further to dissolve a silica monomer into solution according to Eq. (3).



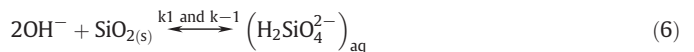
At neutral pH, the solubility limit of silica is low and is reported to be 1.93 and 0.10 mM at 25 °C for vitreous silica and crystalline quartz, respectively [21,22]. At high pH, $\text{Si}(\text{OH})_4$ monomers undergo ionization (Eqs. (4) and (5)) to form highly soluble $\text{SiO}(\text{OH})_3^-$ and $\text{SiO}_2(\text{OH})_2^{2-}$ ions (alternatively written as H_3SiO_4^- and $\text{H}_2\text{SiO}_4^{2-}$) [17]. The solubility of these ions becomes significant at pH values higher than 10 [23].



In addition to the mono-silicic species, larger dissolved silicates such as di-, tri-, and tetra-mers, as well as linear or cyclic oligomers may be present at lower concentrations in the solution (their thermodynamic

data are given in [23–25]). Based on Eqs. (3)–(5), the solubility limit of silica can be calculated as a function of pH, as presented in Fig. 2, which for simplicity considers only three main forms of dissolved species: $\text{Si}(\text{OH})_4$, H_3SiO_4^- , and $\text{H}_2\text{SiO}_4^{2-}$. In calcium-free systems, the dissolved silica remains in the solution and can reach high concentrations up to the solubility limit of alkali silicates.

To study the kinetics of silica dissolution, one can write the dissolution reaction at $\text{pH} > 13$ as Eq. (6), considering that the main dissolved specie at this pH is $\text{H}_2\text{SiO}_4^{2-}$:



The rate of SiO_2 (glass) dissolution can then be written as:

$$r = \frac{d[\text{SiO}_{2(s)}]}{dt} = \frac{1}{2} \frac{d[\text{OH}^-]}{dt} = \frac{d[\text{H}_2\text{SiO}_4^{2-}]_{aq}}{dt} \\ = k_1 [\text{SiO}_{2(s)}][\text{OH}^-]^2 - k_{-1} [\text{H}_2\text{SiO}_4^{2-}] = k_1 [\text{SiO}_{2(s)}][\text{OH}^-]^2 \left(1 - \frac{Q}{K}\right) \quad (7)$$

where k_1 and k_{-1} are the kinetic constants of the forward and reverse reactions, respectively, and $[\text{SiO}_{2(s)}]$ is the mass or surface area of solid

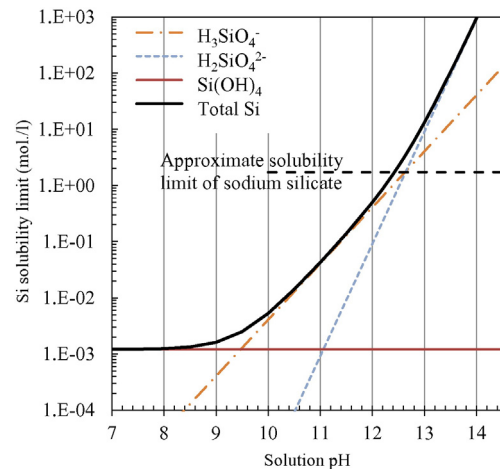


Fig. 2. Speciation graph of vitreous silica at 25 °C using the thermodynamic data presented in Eqs. (3), (4), and (5). Silica solubility increases tremendously with pH.

glass. The equilibrium constant K and the reaction quotient Q are defined as:

$$K = \frac{\{H_2SiO_4^{2-}\}_{EQ}}{\{SiO_{2(s)}\}_{EQ} \cdot \{OH^-\}_{EQ}^2} \quad (8)$$

$$Q = \frac{\{H_2SiO_4^{2-}\}_{aq}}{\{SiO_{2(s)}\}_s \cdot \{OH^-\}^2} \quad (9)$$

where the subscript EQ. indicates equilibrium conditions, and the terms in {} represents activity of the ions. According to Eq. (7), the partial order of the reaction is assumed to be 2 for OH^- and 1 for $SiO_{2(s)}$ and $H_2SiO_4^{2-}$. However, in a more general case, the partial reaction order could be considered as α , β and γ as shown in Eq. (10):

$$r = k_1 \{SiO_{2(s)}\}^\alpha \{OH^-\}^\beta \left(1 - \frac{Q}{K}\right)^\gamma \quad (10)$$

According to Eq. (10), the rate of glass dissolution is related to the pH of the solution and the distance from the equilibrium. In this equation, the surface area of glass can be considered as a proxy for $\{SiO_{2(s)}\}$, which remains constant during the experiments performed in this study.

2.3. Solid products and the role of calcium during glass dissolution

In the presence of dissolved Ca, aqueous silica ions are linked to form poly-metal-silicates (e.g., Eq. (11)) [22,24,26]:



Once a nucleus of critical size is formed, it grows to nano-colloidal silica (sol) through further condensation. Aggregation of these colloidal particles forms larger metal silicate structures, such as gels or precipitates [26]. This mechanism is similar to dissolution of C_2S and C_3S and precipitation of C–S–H, as discussed by [27,28].

In addition to the sol–gel sequence mentioned above, the surface of glass can be altered into a gel layer. This hydrated surface layer can form as a result of ion exchange (leaching) between glass and solution or by breaking some (not all) of the siloxane (Si–O) bonds through hydrolysis [18]. The gel layer (also known as the “passivating reactive interphase, or PRI”) can limit the diffusion of ions between glass and the solution, and as such, reduce the corrosion rate of the underlying glass [29]. Several studies, primarily within the domain of nuclear waste glass research, have looked at formation, composition, and properties of the PRI as a function of the glass and solution compositions, temperature, and glass surface area to solution volume ratio (SA/V) [30–38]. However, most of these studies are based on corrosion of complex multi-oxide nuclear glasses (containing primarily Si, B, Na, and Al) in groundwater (typically $pH < 10$). As such, their findings may or may not be directly applicable to simpler glasses, such as those found in concrete SCMs and aggregates, and at much higher alkalinities.

It has been reported that Ca can reduce the rate of glass alteration, either temporarily or permanently. Oka et al. [36,37] reported an inhibitory effect of Ca, Zn and Al on corrosion rate of fused silica glass in 0.5 M and 1.5 M NaOH solutions, and attributed this to formation of a protective barrier layer. Snellings [10,34] studied dissolution of synthetic Ca–Al–Si glasses at 20 °C and $pH \approx 13$, and confirmed that Ca in the solution can significantly reduce the initial rate of glass corrosion. By studying borosilicate and nuclear glasses, Chave et al. [31] reported that the passivating properties of PRI are enhanced when it contains calcium (originating either from the glass or the solution). Rajmohan et al. [39] studied nuclear glass corrosion at $pH = 7$ to 10, and reported that Ca was retained in PRI, preferably over Na, and this effect increased with

the pH. Further, diffusion coefficient of PRI was lowered by increasing pH. Utton et al. [2,35] measured the dissolution rate of powdered borosilicate glass in saturated $Ca(OH)_2$ solution, and observed a reduced dissolution rate due to formation of calcium borate and other Ca- and Mg-bearing precipitates on the surface of glass.

By studying borosilicate glasses, Mercado-Depierre et al. [32] illustrated that both pH and the glass surface area to solution volume ratio (SA/V) affect the nature of Ca interaction with silica surface in a corrosion experiment. At high pH (≈ 11.7) and low SA/V, Ca is integrated into PRI and mitigates glass corrosion. However, at high SA/V, alteration of glass is accelerated in the presence of Ca, due to conversion of glass to C–S–H with Ca/Si ≈ 0.85 (similar to pozzolanic reaction). Fournier et al. [33] stated that although the rate of glass alteration drops with time due to formation of PRI, a resumption of alteration rate is possible. This is more probable in systems with high SA/V (e.g., confined media), and is due to formation of secondary crystalline phases such as zeolite (in systems containing Al) and C–S–H (in systems containing Ca) [32,40].

2.4. Use of soda lime glass in concrete

Recycled soda-lime glass (from recycling glass bottles and window plates) has been considered in past studies as a potential pozzolan [1, 41–45] or aggregate [46–48] for concrete. Rajabipour et al. [49,50] showed that glass aggregates larger than approximately 0.6 mm undergo deleterious ASR, which originates through pre-existing internal microcracks of crushed glass particles (Fig. 3a). The surface of glass aggregates exposed to cement paste was apparently immune to ASR and was primarily subjected to a pozzolanic reaction (Fig. 3b). The internal microcracks originated during glass crushing before its use in concrete, and were found to be more extensive in larger particles [51]. It was also confirmed that these residual cracks could be removed through annealing of crushed glass cullet to mitigate ASR [51]. Similarly, when using crack-free soda-lime glass beads in portland cement mortars, no ASR was observed (Fig. 3c). An intriguing question is why glass particles do not undergo ASR at their surface, and what role, if any, the presence of solid $Ca(OH)_2$ at the glass–cement paste interface plays in preventing ASR. Interestingly, when soda-lime glass aggregates were used in alkali-activated fly ash mortars, which do not form solid $Ca(OH)_2$, ASR gel was observed both within the interior and at the surface of glass aggregates (Fig. 3d). It should be noted that soda-lime glass contains approximately 7 to 10% CaO, which supplies Ca necessary for formation of ASR gel.

3. Materials and experimental methods

This study was divided in two phases (Table 1). First, the kinetics of glass dissolution in highly alkaline NaOH solutions ($12.0 < pH < 14.9$) in the absence or presence of Ca was evaluated. In the second phase, solid products that form as a consequence of soda-lime glass dissolution were characterized. Two types of silicate glasses were studied: a soda-lime (SL) and a fused silica (FS) glass. Table 2 shows the oxide composition of these two glasses. Glass dissolution experiments were conducted in static batch reactors, where two SL glass slides ($50 \times 75 \times 1$ mm) were submerged in NaOH solutions in properly sealed plastic containers to obtain $SA/V = 45 \text{ m}^{-1}$. Attempts were made to minimize carbonation by preparing the solutions in a N_2 purged glove box, and minimizing the exposure of the materials to the atmosphere. The setups were stored in an oven at 60 °C or otherwise noted temperatures. The fused silica slides had smaller width (25 mm); however, the SA/V was maintained at 45 m^{-1} . Reagent NaOH and $Ca(OH)_2$ were mixed with deionized (DI) water in preparation of the solutions.

3.1. Kinetics of silica glass dissolution in NaOH solutions

3.1.1. Effect of NaOH concentration (or pH) on dissolution rate

As the first parameter, the effect of NaOH concentration (from 0.01 to 8.0 M) on dissolution rate of SL glass was studied. After 7 days, slides

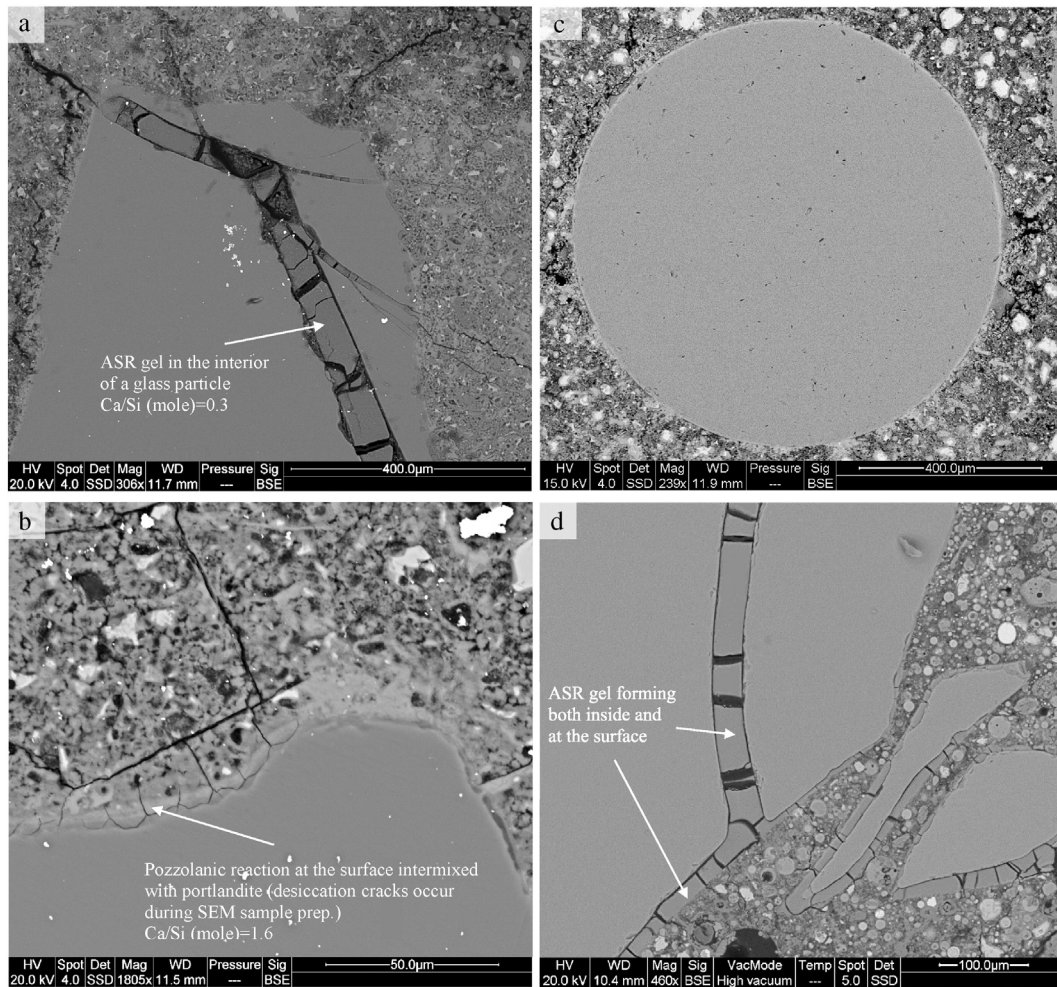


Fig. 3. BSE images of mortars containing soda-lime glass: (a) ASR gel formation in the interior of glass particle while the surface remains immune, (b) pozzolanic reaction at the glass-cement paste interface, (c) absence of ASR in crack-free glass beads, (d) ASR in alkali activated fly ash mortar occurring both at the surface and interior of glass.

were removed from the solutions, thoroughly washed with water, dried, and weighed using a scale with the precision of 0.0001 g, to quantify the mass loss for each slide. As discussed below, after washing, no residual precipitates remained on the surface of glass. As such, mass measurements represent the true mass loss of glass due to alkaline corrosion. After finding the most corrosive NaOH solution (i.e., 1.0 M as will be seen in the following sections), the remaining experiments were performed with this solution (Table 1).

Table 1

Experimental plan that was followed in this research; all glass dissolution experiments were at 60 °C, except for the analysis of the temperature effect.

	Glass type	Solution
<i>Phase I: kinetics experiments</i>		
Effect of pH on glass dissolution rate	SL	NaOH (0.01–8.0 M) (without Ca)
Effect of temperature on glass dissolution rate	SL	1.0 M NaOH (without Ca)
Effect of dissolved Ca on glass dissolution rate	SL and FS	1.0 M NaOH (with and without Ca)
ICP analysis of the solution	SL and FS	1.0 M NaOH (with and without Ca)
<i>Phase II: characterization of solid products</i>		
(E)SEM-EDS	SL	1.0 M NaOH
XRD	SL	(with and without Ca)
N ₂ adsorption	SL	
FIB-TEM	SL	

3.1.2. Effect of temperature on dissolution rate

SL slides were submerged in 1 M NaOH solutions at 20 °C, 40 °C, 60 °C and 80 °C. The mass loss values were measured up to 210 days in experiments at 20 °C and 40 °C, up to 46 days at 60 °C, and up to 14 days at 80 °C. The activation energy of SL glass dissolution in 1 M NaOH solution was determined using the Arrhenius equation (Eq. (12)); where r is the mass loss rate, A is a pre-exponential factor, E_a is the activation energy of dissolution, R is the universal gas constant (8.314 J/mol·K), and T is the absolute temperature.

$$r = A e^{\frac{-E_a}{RT}} \quad (12)$$

3.1.3. Effect of dissolved Ca on dissolution rate

To examine how the presence of calcium influences the rate of glass dissolution, the following four systems were studied:

1. SL glass in 1 M NaOH solution, without added Ca(OH)₂ (labeled “soda-lime No-CH”),

Table 2

Oxide composition (wt.%) of soda-lime and fused silica glass slides.

	SiO ₂	CaO	Na ₂ O	Al ₂ O ₃	MgO	K ₂ O
Soda-lime glass (SL)	73.8	7.8	12.3	0.9	3.9	0.9
Fused silica glass (FS)	>99.9	–	–	–	–	–

- SL glass in 1 M NaOH solution, under saturated with respect to $\text{Ca}(\text{OH})_2$ (labeled “soda-lime US-CH”),
- SL glass in 1 M NaOH solution, saturated with and also containing excess residual $\text{Ca}(\text{OH})_2$ solid powder in the reactor (labeled “soda-lime SS-CH”),
- FS glass in 1 M NaOH solution without $\text{Ca}(\text{OH})_2$ (labeled “fused silica No-CH”).

The “fused silica No-CH” system contained practically no calcium. The “soda-lime No-CH” system only contained calcium that was contributed by dissolution of the SL glass structure (7.8% CaO). The “soda-lime US-CH” system was prepared by filtering a $\text{Ca}(\text{OH})_2$ saturated 1 M NaOH solution, and diluting it with adding more 1 M NaOH solution. For “soda-lime SS-CH” system, 1.0 g of $\text{Ca}(\text{OH})_2$ powder was mixed in 0.33 l of 1 M NaOH solution. Since the solubility of $\text{Ca}(\text{OH})_2$ in 1 M NaOH is very low (approximately 0.45 mM = 18 mg/l), most of the $\text{Ca}(\text{OH})_2$ precipitated to maintain a solution saturated with $\text{Ca}(\text{OH})_2$ throughout the experiment. Mass loss of glass slides in these four systems was measured after 7, 14, 21 and 28 days of exposure to the solutions. This led to 16 independent reactors to avoid mass loss measurement at each age to interfere with measurements at later ages for the same system.

Exposure of SL glass to 1 M NaOH solution resulted in formation of altered layer and solid products on the surface of glass that could be easily removed under running water to leave a transparent surface (Fig. 4-left). However, in the presence of added $\text{Ca}(\text{OH})_2$ (i.e., “soda-lime SS-CH” system) the altered layer (rich in Ca) was strongly-bonded, and could not be removed by washing with water, and therefore left a translucent surface (Fig. 4-right). This surface layer could interfere with mass loss measurements to correctly quantify the dissolution rates. To address this challenge, after the dissolution experiment, the surface layer was removed by dissolving it in 6.0 M hydrochloric acid. SEM analysis confirmed that submerging the slides in acid for 1 h completely removed the precipitated layer. This practice was checked separately on a plain SL glass to ensure that the substrate glass is not losing mass during exposure to the acid. For the “fused silica No-CH” system, no corrosion products were formed and the surface of the slides remained transparent (Fig. 4-middle). However, during the 3rd week of the exposure, the edges of the slides started to crack and scale. This influences the mass loss results, which is discussed later.

3.1.4. Analysis of the solution chemistry

The alkaline solution surrounding glass slides in the four systems introduced in Section 3.1.3 was periodically sampled and filtered using 0.2 μm PTFE filter syringes. The solution pH was measured by acid titration and was found to remain near 14.0 throughout the course of the

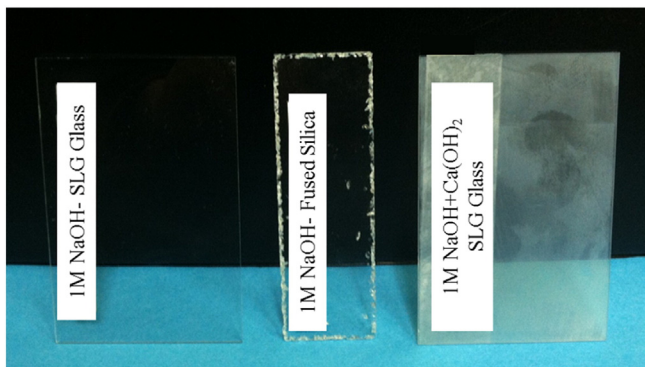


Fig. 4. Left: soda-lime glass exposed for 14 days to 1 M NaOH in the absence of $\text{Ca}(\text{OH})_2$ (soda-lime No-CH system); middle: Fused silica glass exposed for 28 days to 1 M NaOH; right: Soda-lime glass exposed for 14 days to 1 M NaOH saturated with $\text{Ca}(\text{OH})_2$ (soda-lime SS-CH system); all slides are washed after exposure.

experiment. Also, the concentration of Ca and Si were measured using inductively coupled plasma atomic emission spectrometry (ICP-AES) up to 80 day of exposure. Prior to measurement, ICP samples were diluted 10 \times using 2% HNO_3 solution.

3.2. Characterization of the corrosion products

3.2.1. SEM/EDS analysis

Scanning electron microscopy coupled with energy dispersive spectroscopy (SEM/EDS) was employed to analyze the corrosion products of SL glass. After 1 and 2 weeks of exposure to 1 M NaOH solution at 60 $^{\circ}\text{C}$, glass slides were removed from the solutions and dried under vacuum. Some slides were alternatively rinsed prior to drying. One slide was carefully broken and a small piece was placed on a vertical sample holder for cross-sectional analysis. In addition, the products were collected from the surface of SL slides and gently spread on a carbon tape. High vacuum field emission SEM (FEI NanoSEM 630) was employed to study the microstructure and composition of these products. EDS data was generated on at least 10 area zones or spots for each observed feature.

Furthermore, to ensure that the observed microstructural features were not the artifacts of drying or high vacuum conditions in SEM, the products in “soda-lime No-CH” system were also studied in a low vacuum mode of an environmental SEM (FEI Quanta 200). SL slides were removed from the solutions, promptly broken and a piece was placed horizontally inside the ESEM chamber, which was later adjusted to one of two conditions: “T = 20 $^{\circ}\text{C}$ and RH = 95%” or “T = 25 $^{\circ}\text{C}$ and RH = 80%”. The surface of the glass piece was slightly disturbed in randomly selected zones to better observe the microstructure of the corrosion products.

3.2.2. XRD analysis

Corrosion products of soda-lime glass after exposure to 1 M NaOH solution (with and without $\text{Ca}(\text{OH})_2$) were analyzed using powder X-ray diffraction (XRD). After 1, 2 and 3 weeks of exposure, corrosion products were collected from vacuum-dried slides, ground into a powder, and placed on a zero background zirconium holder. Diffraction patterns were collected using a PANalytical X’Pert Pro MPD horizontal goniometer with Cu-K α radiation, and fixed slit incidence and diffracted optics (0.5 $^{\circ}$ anti-scatter, 0.02 mm nickel filter). Data was collected at 45 kV and 40 mA from 5 to 70 degrees 2θ for duration of ~30 min. For the specimen “soda-lime No-CH” at 2 weeks, a beam knife was used to improve the reflectivity curves, specifically at low 2θ angles. Resulting patterns were analyzed using Jade software (MDI, Livermore, CA).

3.2.3. N_2 adsorption porosity measurement

Nitrogen absorption analysis was employed to quantify the porosity, pore size distribution, and BET surface area of the corrosion surface products after 1 week of the experiment. A comparison was made between the products that formed in the absence or presence of $\text{Ca}(\text{OH})_2$ in the solution (“soda-lime No-CH” vs. “soda-lime SS-CH”). Corroded glass slides were rinsed gently using DI water, and dried under vacuum for 7 days. Next, the corrosion products were carefully collected from the surface of each slide using a blade and placed inside BET chamber. N_2 adsorption isotherms were obtained using Micromeritics ASAP 2020 instrument.

3.2.4. TEM analysis of corroded glass surface

To better understand the mechanism of glass dissolution and to study the interface between the glass and corrosion products, thin sections were prepared for transmission electron microscopy (TEM), using focused ion beam (FIB) method. A soda-lime No-CH slide, after corrosion for 7 days in 1 M NaOH solution was vacuum dried. Inside a SEM-FIB chamber, starting from the top of the corrosion products, a square area was chosen for ion milling. First, a thin layer of platinum (Pt) was deposited as a line in the middle of the square area to protect the

specimen directly underneath the Pt-line from ion milling. Next, using Ga^+ ions, two trenches were milled at the two sides of the Pt line to create a vertical slab composed of the Pt-deposit, corrosion products, and the glass substrate. By progressively reducing the ion beam's current and spot size, the slab was milled to a thin section of approximately 50 nm. The process is shown in Fig. 5. Using a manipulator needle, the thin section was placed on a TEM grid. Due to the challenges involved in this approach (will be discussed later), the second specimen (soda-lime SS-CH slide) was prepared slightly differently. Glass slide was dried and broken after two weeks of exposure and FIB was initiated from the cross section of glass as shown in Fig. 5c. TEM imaging was performed using a JEOL 2010F TEM operated at 200 kV.

4. Results

4.1. Kinetics of silica glass dissolution

4.1.1. Effect of NaOH concentration on dissolution rate

Fig. 6 shows that increasing NaOH concentration up to 1 M resulted in an increased rate of SL glass dissolution ($\text{mg}/\text{cm}^2\cdot\text{day}$). However, for higher molarities, the rate of dissolution decreased. Tarnopol and Junge [52] also observed that dissolution rate of SL glass was maximized at an intermediate concentration for NaOH and Na_2CO_3 solutions of approximately 1.3 M. It should be noted that in this SA/V system, dissolution of SL slides was found to continue at a nearly constant rate (Fig. 7a) until the entire glass slide is consumed. According to Fig. 6, for $\text{pH} < 14$, the

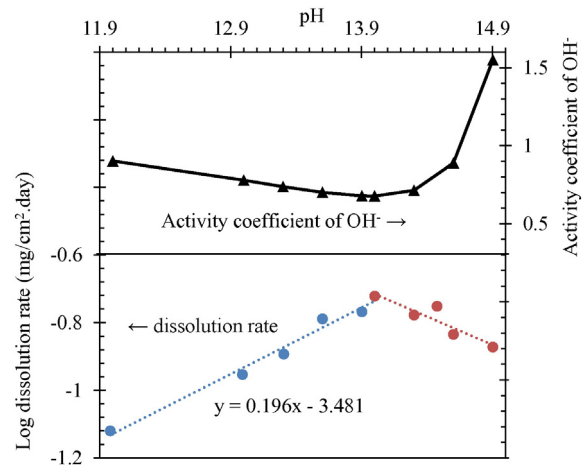


Fig. 6. Dissolution rate of soda-lime glass in NaOH solutions of different pH values at 60°C (lower part of the graph – left axis), and activity coefficient of OH^- in the same solutions (upper part of the graph – right axis), calculated based on the Bromley model [48].

logarithm of the dissolution rate followed a linear trend versus the pH of the solution:

$$\log[\text{r} \equiv \text{SL glass dissolution rate } (\text{mg}/\text{cm}^2\cdot\text{day})] = 0.196 \text{ pH} - 3.481 \quad (13)$$

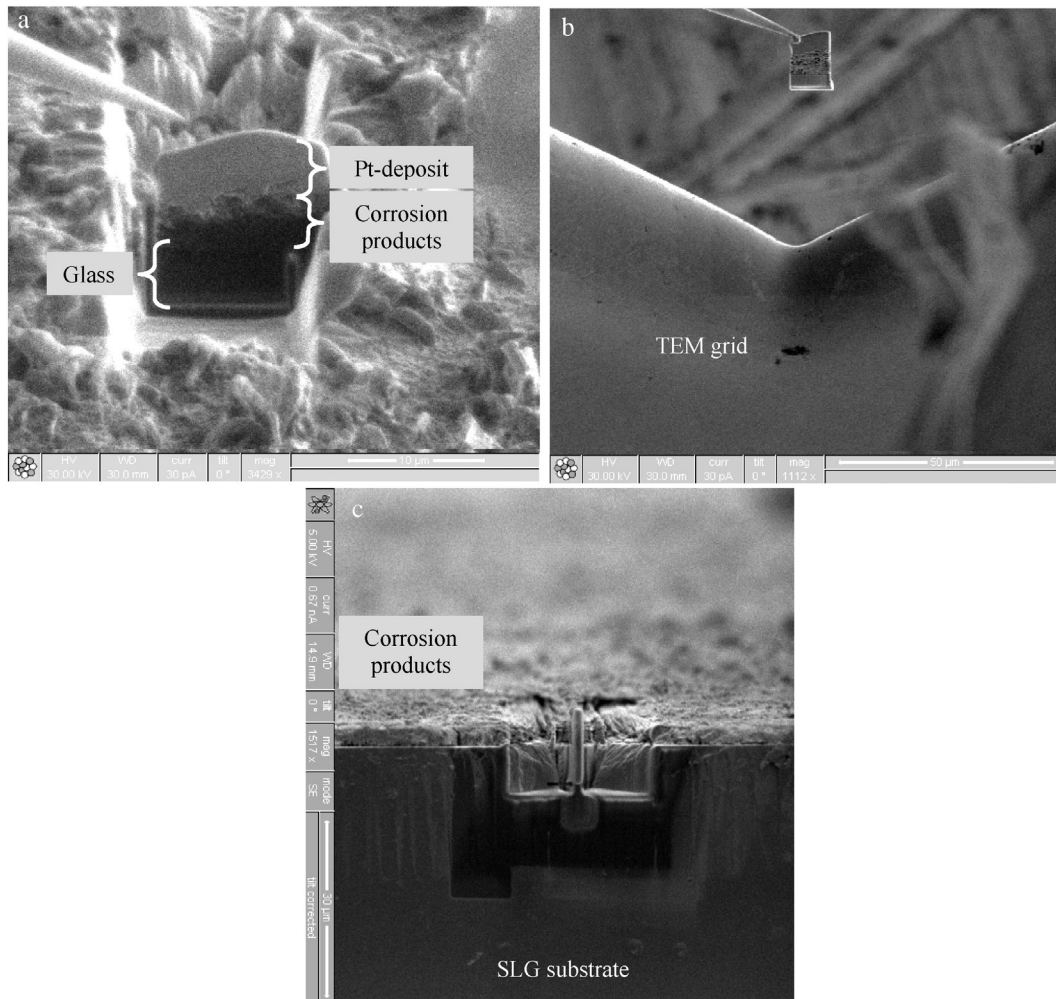


Fig. 5. FIB process showing (a) milling from the top and through porous precipitates in soda-lime No-CH system, (b) placement of thin section on TEM grid, and (c) milling through a cross section on soda-lime SS-CH system.

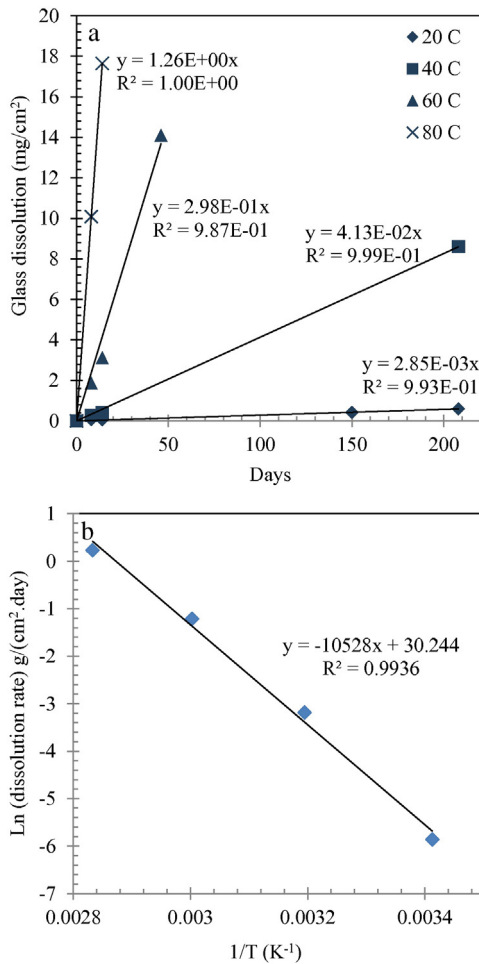


Fig. 7. (a) SL slide dissolution mass loss in 1 M NaOH solution (No-CH) at different temperatures, (b) linear correlation between Ln (dissolution rate) versus 1/T to obtain the activation energy.

According to Eq. (10), the slope of this line is the partial order of dissolution reaction with respect to $[\text{OH}^-]$: $\beta \approx 0.20$. Note that in Eq. (10), the value of Q/K approaches zero since the concentration of the dissolved silica at this age (7 d) was much below the saturation limit at this pH (compare Figs. 9a and 2). In addition, the surface area of glass slides $[\text{SiO}_{2(s)}]$ remained approximately constant during the experiment.

The observation that SL glass dissolution rate decreased at very high $\text{pH} > 14$ may be attributed to the increased negative electric charge on the glass surface, due to formation of $\equiv\text{S}-\text{O}^-$ sites. In addition, $\text{H}_2\text{SiO}_4^{2-}$ ions would accumulate near the glass surface, which repel the attacking hydroxyl ions. Another hypothesis is that at very high NaOH concentrations, overcrowding and strong ion-ion interactions could decrease the affinity of the solution to dissolve silicates. In such concentrated solutions, water activity is decreased and there may not be enough water molecules to fully hydrolyze the ionic species; and this may hamper the dissolution rate. This phenomenon also manifests itself in an increased activity coefficient of OH^- ions above $\text{pH} = 14$ (Fig. 6), as calculated based on the Bromley's model for strong electrolyte solutions [53]. Finally, due to the static nature of the experiment, and low self-diffusion coefficients of ions in concentrated solutions [54], dissolved silicates accumulate in the vicinity of glass surface. This reduces the glass dissolution rate by intensifying the previous mechanisms. These hypotheses need further verification to draw firm conclusions.

4.1.2. Effect of temperature on dissolution rate

Fig. 7a shows that the mass loss of SL glass changes approximately linearly with respect to time (constant rate), which agrees with Eq. (10). This is due to the low concentration of dissolved silica comparing to the saturation limit; i.e., $Q/K \approx 0$ (compare Figs. 9a and 2), and the fact that glass surface area $[\text{SiO}_{2(s)}]$ and pH remained constant during the corrosion experiment.

Using the Arrhenius equation (Eq. (12)), the activation energy of SL glass dissolution in 1 M NaOH solution was calculated as $87.5 \text{ kJ} \cdot \text{mol}^{-1}$ (Fig. 7b). This relatively high value of activation energy indicates that the dissolution is a chemically-controlled surface reaction, and formation of a surface corrosion products layer did not impose a diffusion barrier against dissolution of SL glass in No-CH system. Activation energy of dissolution is a pH-dependent parameter, which for example, was reported to vary from 43 to $96 \text{ kJ} \cdot \text{mol}^{-1}$ for dissolution of quartz at $\text{pH} = 4$ and 11, respectively [55]. Frugier et al. [18] reported an activation energy of $76 \text{ kJ} \cdot \text{mol}^{-1}$ for dissolution of SON68 nuclear glass at temperatures ranging from 25 to 100°C and $\text{pH} = 6$ to 10.

4.1.3. Effect of dissolved Ca on dissolution rate

The presence of dissolved Ca had a remarkable impact on reducing the dissolution rate of silica glass at high pH. Fig. 8a compares the dissolution mass loss of SL glass in 1 M NaOH solution that was saturated with $\text{Ca}(\text{OH})_2$ versus the solution that did not contain $\text{Ca}(\text{OH})_2$. It should be reminded that in the SS-CH reactor, a strongly bonded layer of corrosion products formed on the surface of glass slides during the

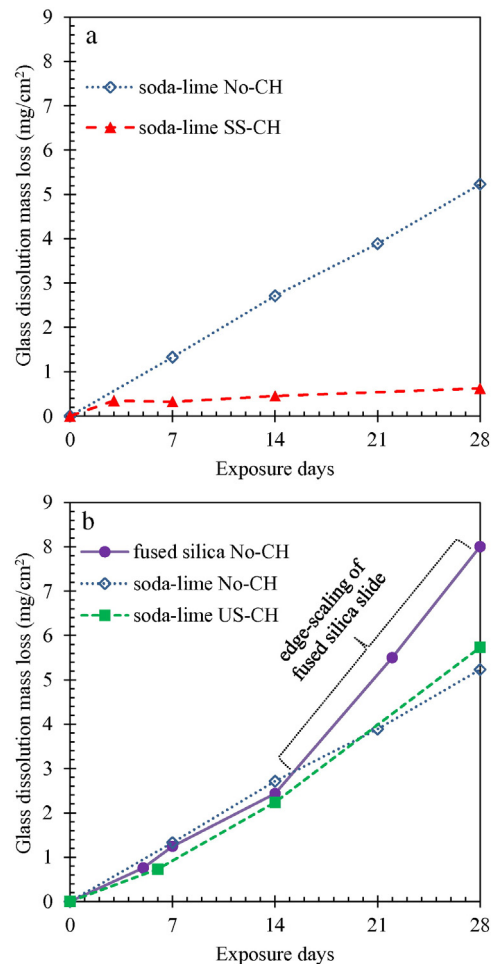


Fig. 8. (a) Dissolution mass loss of glass is remarkably reduced in reactors saturated with portlandite (SS-CH) in comparison with No-CH. Precipitate layer was removed prior to mass measurements. (b) Dissolution rate is comparable in reactors undersaturated or without CH. All experiments performed in 1 M NaOH solution at 60°C .

experiment; but this layer was removed using HCl acid prior to mass measurements. As noted before, SEM imaging and parallel treatments of virgin glass confirmed that the acid treatment employed, effectively dissolved the corrosion product layer without dissolving the substrate glass. Comparison of the glass dissolution between the two reactors (Fig. 8a) show that the dissolution rate was initially similar in both reactors. However after 3 days, the dissolution rate was drastically reduced in the SS-CH reactor. This is likely attributed to the formation of a dense and protective layer on the surface of glass. The characterization results provided in Section 4.2 identify this layer to be primarily C-S-H. According to Chave et al. [31] calcium from the solution enhances condensation of siloxane bonds and modifies the passivating property of the altered layer on the glass surface.

As seen in Fig. 8b, the SL dissolution rate in the US-CH reactor was similar to that of the No-CH reactor. The Ca concentration in both reactors was likely to be insufficient (and was rapidly consumed; confirmed by ICP-AES) to form a dense protective layer on the surface of glass. Fig. 8b also shows that dissolution of fused silica slides appeared to be similar to that of SL glass up to 14 days. However after this time, edge cracking and scaling started to appear on the slides (Fig. 4-middle), which increased their mass loss. As such, mass measurements of FS slides were only reliable up to 14 days. The reason for this scaling is unclear, but might be due to the procedure used for cutting FS slides that resulted in residual stresses and micro-cracks at the edges. These microcracks could propagate and scale off under the alkaline attack.

4.1.4. The solution chemistry

According to Fig. 9a, No-CH and US-CH systems showed very similar values of silica release into the solution. An approximate mass balance calculation using glass slide mass loss and ICP data suggests that more than 80% of the dissolved Si went into the solution, and the rest was consumed in formation of solid corrosion products. On the other hand, in the SS-CH system, concentration of Si in the solution was measured to be very low, which is likely due to its reaction with Ca to form C-S-H on the surface of glass slide. The fused silica No-CH system showed the highest Si concentration in the solution, which is reasonable because: (a) FS has higher SiO₂ content than SL glass, resulting in a higher Si release at the same glass dissolution rate, (b) Si in FS reactor remains entirely in the solution due to the absence of Ca and lack of precipitate formation, and (c) FS glass experienced an increased surface area due to edge scaling beyond 14 days of corrosion.

The Ca concentration (Fig. 9b) corroborates the above observations. In the SS-CH solution, Ca concentration remained near saturation due to the presence of solid Ca(OH)₂ in the reactor. The small decrease in Ca concentration with time may be due to a slight increase in the pH of the solution, which reduces the solubility of Ca(OH)₂. In No-CH and US-CH soda-lime reactors, similar trends of initially increasing Ca concentration due to dissolution of SL glass, followed by decreasing Ca concentration was observed. The reduction could be the result of reaction with dissolved silica to form solid products.

4.2. Characterization of the corrosion products

4.2.1. SEM/EDS results

Two types of corrosion products were observed to form on the surface of glass slides in the “soda-lime No-CH” reactors (Fig. 10a). One type appeared as ordered pillars extending perpendicular to the surface of glass, and the other being a more porous and randomly oriented products, forming on top of the ordered layer. The Ca/Si ratio in each phase is also presented (measured by EDS for solid phases and ICP for the solution). It was observed that the corrosion products had 6 to 9 times higher Ca/Si than the source SL glass. In combination with the ICP results (Fig. 9) and considering that SL glass is the only source of Ca in this reactor, it can be argued that the majority of Si (>80%) from the dissolving glass was passed into the solution, while Ca was bound in the solid products.

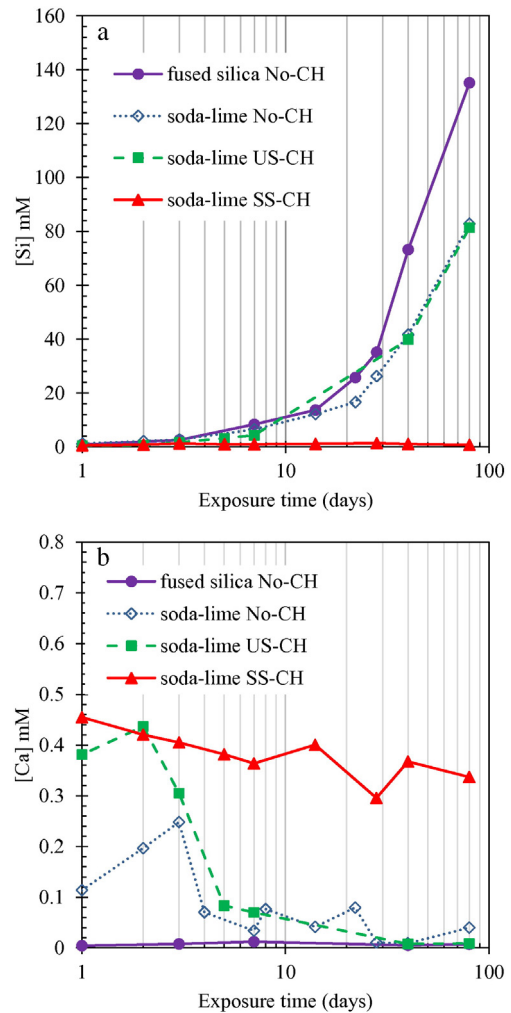


Fig. 9. Changes in the concentration of (a) Si, and (b) Ca in the reactor solutions as a function of time.

Fig. 10b shows the morphology of the ordered products, when collected from the surface of a rinsed SL slide. It can be observed that the ordered layer is highly porous, with a honeycomb morphology. Note that the top surface of the ordered products seen in Fig. 10b was facing the glass substrate. Fig. 10c shows the microstructure of the disordered products. These have a morphology and Ca/Si close to that of tobermorite (a crystalline form of C-S-H) [56,57], and were identified as such by XRD analysis (Section 4.2.2).

Formation mechanism of the glass corrosion products deserves attention. The products could precipitate from the solution or could form by an in-situ alteration of the glass surface [14,30]. The disordered nature of the outer products and the fact that they have formed on top of the ordered products suggest that these have likely precipitated from the solution. This agrees with the initial increase and the subsequent decrease of Ca concentration in the solution (Fig. 9b). They resemble the outer C-S-H products formed during cement hydration. The ordered products, however, are more likely to be the result of in-situ transformation of glass or dissolution-precipitation reactions at the nano-scale. This is discussed further by the TEM results. It is likely that the boundary between the ordered and disordered products was the initial surface of soda-lime glass.

Figs. 11 (a) and (b) show the microstructure of the corrosion products, imaged by ESEM at $T = 20^\circ\text{C-RH} = 95\%$ and $T = 25^\circ\text{C-RH} = 80\%$, respectively. The right side of Fig. 11a shows the top view of the disordered precipitates. The left side of the image shows the surface that was disturbed using a sharp blade to reveal the ordered products

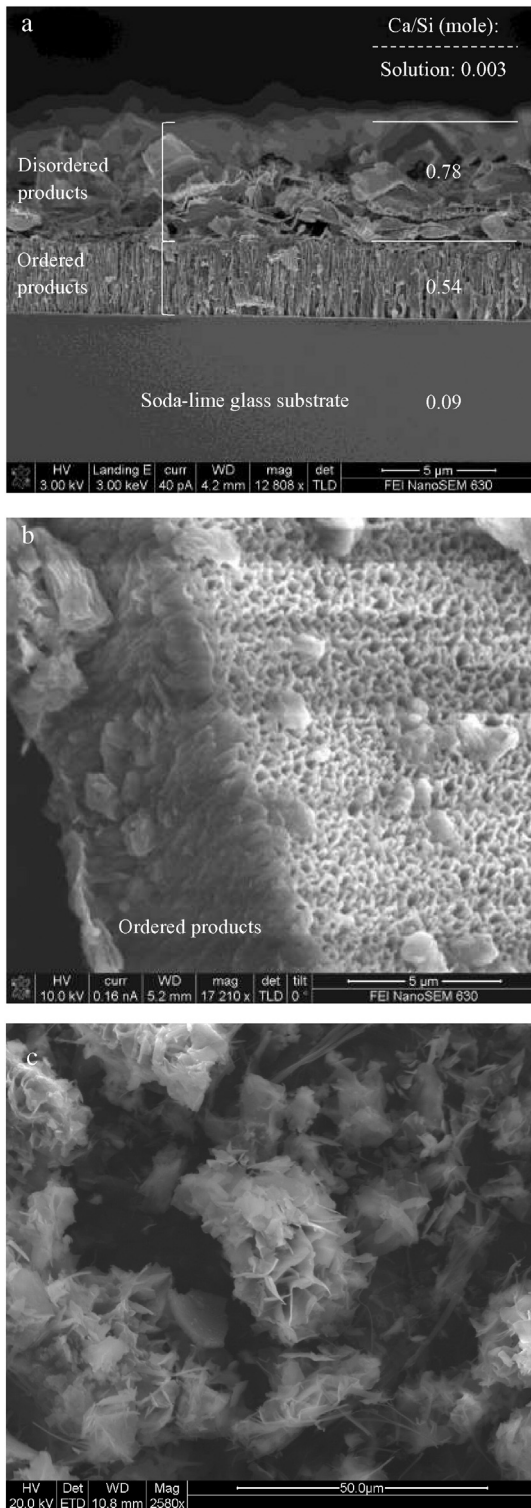


Fig. 10. (a) Two types of corrosion products were formed on the surface of soda-lime glass in the No-CH reactor; (b) ordered (inner) corrosion products after rinsing and removing the (c) disordered (outer) products. Image “a” was taken after 1 week corrosion, while “b” and “c” correspond to 2 weeks corrosion in 1 M NaOH at 60 °C.

underneath. Fig. 11b also shows the microstructure of the products, confirming that these products formed during corrosion of the glass inside the NaOH solution and not as a result of drying or high vacuum SEM.

In the reactors saturated with portlandite (SS-CH), both ordered and disordered corrosion products were also formed. However, unlike the

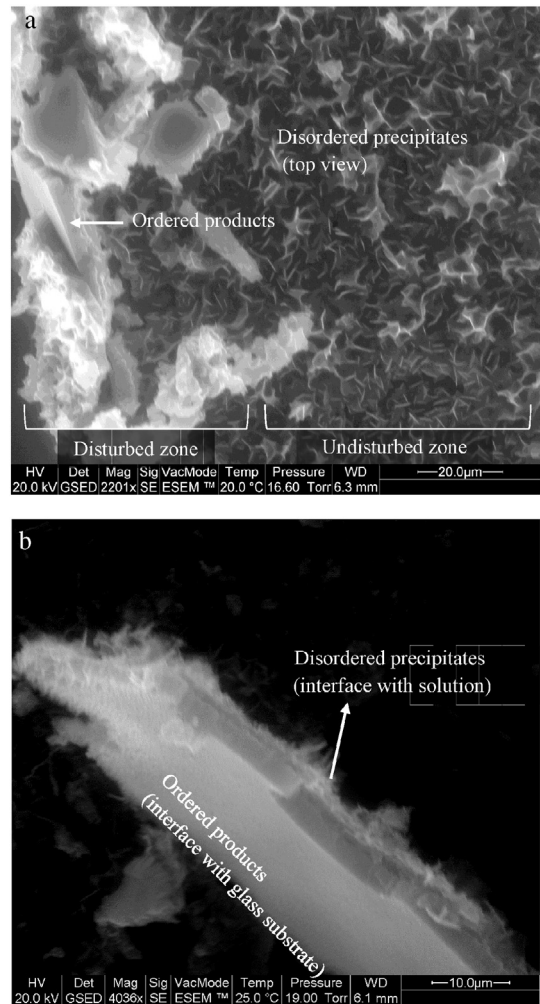


Fig. 11. Corrosion products in the “soda-lime No-CH reactor” imaged by ESEM at (a) T = 20 °C, RH = 95% and, (b) T = 25 °C, RH = 80%. Images correspond to corrosion in 1 M NaOH at 60 °C for 1 week.

No-CH reactors, the ordered products had high Ca, appeared to be denser (also confirmed by the N₂ adsorption results), and were strongly bonded to the substrate glass. Fig. 12 shows a SEM image and X-ray maps of Si, Ca, and Mg within the substrate SL glass and the ordered surface layer. The disordered precipitates were rinsed away using DI water prior drying and imaging.

Table 3 presents the elemental composition of the corrosion products of SL glass in the presence or absence of calcium. It should be noted that since these EDS data were not acquired on flat surfaces, the results should be treated qualitatively rather than drawing firm quantitative conclusions. Based on the EDS results, the corrosion products are primarily hydrated calcium (and possibly magnesium) silicates, with smaller contents of Na and Al. ICP of Ca and Mg (not included) showed a very low concentration of these elements in the solution (except for the [Ca] in SS-CH reactor), suggesting that both Ca and Mg react preferentially with the dissolved silica to form the solid corrosion products. It is more meaningful to compare the relative ratio of the elements (e.g., Ca/Si), rather than their absolute values. In the No-CH reactor, the average Ca/Si of all corrosion products was 1.05 on a weight basis. In comparison, corrosion products in the SS-CH reactor, had a considerably higher Ca/Si (1.84), and considerably lower Na/Si (0.05 vs. 0.22) and Mg/Si (0.31 vs. 0.59). Due to its divalent nature, Ca acts as a pseudo network former and increases the stability of hydrated silicates [6]. On the other hand, Na is monovalent and breaks up the silica network by forming non-bridging oxygens. As a result, hydrated calcium silicates

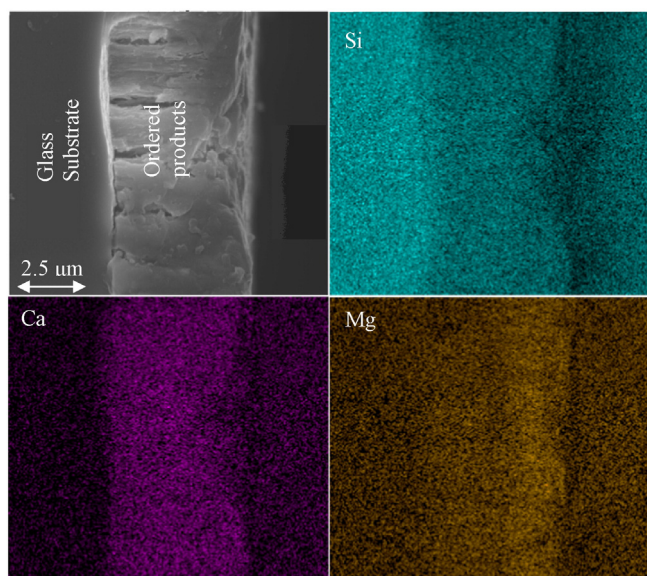


Fig. 12. SEM and X-ray EDS maps of soda-lime glass and ordered (inner) corrosion products in the SS-CH reactor after 2 weeks exposure to 1 M NaOH at 60 °C. Disordered (outer) precipitates were rinsed away prior to imaging.

with higher Ca and lower Na have been suggested to be stronger, stiffer, and more volumetrically stable [58–61]. This is likely the reason that the corrosion products layer in the SS-CH reactor was strongly bonded to the substrate glass, while the products in the No-CH reactor could be easily removed from the glass surface.

4.2.2. XRD results

Fig. 13 shows X-ray diffraction patterns of the corrosion products (mixture of both ordered and disordered) of SL glass in No-CH and SS-CH reactors. The main crystalline phase in the corrosion products was calcium silicate hydrates (C-S-H), identified as plombierite (14 Å tobermorite $\text{Ca}_5\text{Si}_6\text{O}_{16}(\text{OH})_2$) [56,62,63]. The diffuse peak at approximately $2\theta \sim 7.1^\circ$ corresponds to the basal spacing between C-S-H layers, and can be measured as approximately 12.44 Å, which is slightly smaller than plombierite (14 Å). The interlayer spacing depends on the degree of hydration of C-S-H and temperature [62]. In addition to C-S-H, brucite ($\text{Mg}(\text{OH})_2$) was identified as a minor phase. Although no Na-bearing mineral was identified in XRD, it is likely that Na is absorbed within C-S-H. In general, agreement between XRD and EDS results was satisfactory. A phase with corresponding peaks at 11.2° and 22.4° could not be identified confidently. An amorphous hump within the 2θ range of $28\text{--}36^\circ$ is attributed to the amorphous C-S-H and is more profound in SS-CH system, which is due to the higher Ca content within

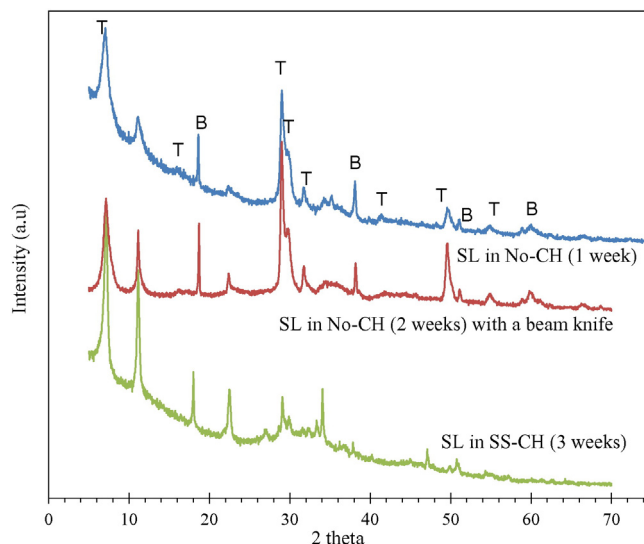


Fig. 13. XRD patterns identifying the crystalline corrosion products as tobermorite C-S-H (T) and brucite (B). The SS-CH reactor also shows amorphous C-S-H hump.

C-S-H chains [57]. The nature of the corrosion products did not significantly change with time.

4.2.3. N_2 adsorption results

The BET surface area of the corrosion products in soda-lime SS-CH and No-CH systems were measured as 51.2 and 32.4 m^2/g , respectively. The pore size distributions are shown in Fig. 14, suggesting that corrosion products in the SS-CH reactor had lower porosity and smaller pore size. In this reactor, pores smaller than 100 Å constituted more than 85% of the total volume of the pores, and no pores smaller than 20 Å was measured. For No-CH system, the pores smaller than 100 Å constituted only 32% of the total volume of the pores. It should be noted that pore size distribution measurements using N_2 adsorption becomes inaccurate for pore sizes larger than 300 to 400 Å [64,65].

4.2.4. TEM results

Analysis of the thin sections of the soda-lime No-CH slide, prepared using the first FIB approach (Fig. 5a) showed significant damage and extensive re-deposition of Pt and Cu on the specimen. Initiation of ion milling through the porous and weakly bonded corrosion products, made it difficult to obtain a suitable thin section for TEM analysis. In the second FIB approach, which was applied to the soda-lime SS-CH slide, milling was initiated from a cross section of glass (Fig. 5c) and the corrosion products were strongly bonded to the glass surface. As such, a much better thin section was obtained.

Table 3
EDS elemental composition (wt.%) of soda-lime glass and its corrosion products in “No-CH” reactor after 1 week, and in “SS-CH” reactor after 2 weeks exposure to 1 M NaOH at 60 °C. Each column is an average composition ± 1 standard deviation determined from EDS analysis of at least ten areas on a given material.

	Original soda-lime glass	Soda-lime No-CH reactor			Soda-lime SS-CH reactor
		Ordered products	Disordered products	Average of all products ^a	Average of all products ^a
O	46.1 \pm 0.6	38.2 \pm 3.3	49.8 \pm 3.6	41.4 \pm 0.6	39.9 \pm 1.0
Si	35.6 \pm 1.9	16.3 \pm 4.2	18.7 \pm 2.1	19.8 \pm 1.2	18.5 \pm 2.2
Na	9.4 \pm 1.4	6.1 \pm 3.2	6.4 \pm 4.0	4.3 \pm 1.9	0.89 \pm 0.6
Ca	4.9 \pm 0.1	12.6 \pm 3.1	17.7 \pm 2.5	20.9 \pm 3.7	33.4 \pm 3.4
Mg	2.8 \pm 0.1	6.1 \pm 3.2	4.4 \pm 3.9	11.6 \pm 1.1	5.8 \pm 2.0
Al	0.7 \pm 0.1	2.3 \pm 0.1	2.2 \pm 0.8	1.7 \pm 0.3	1.4 \pm 0.6
K	0.8 \pm 0.1	N/D	N/D	N/D	N/D
Ca/Si (wt)	0.14	0.78 \pm 0.09	1.12 \pm 0.13	1.05 \pm 0.14	1.84 \pm 0.32
Ca/Si (mole)	0.09	0.54 \pm 0.06	0.78 \pm 0.8	0.73 \pm 0.09	1.28 \pm 0.22

^a Average of all products was obtained from EDS analysis on larger areas on collected corrosion products, which contains both ordered and disordered products.

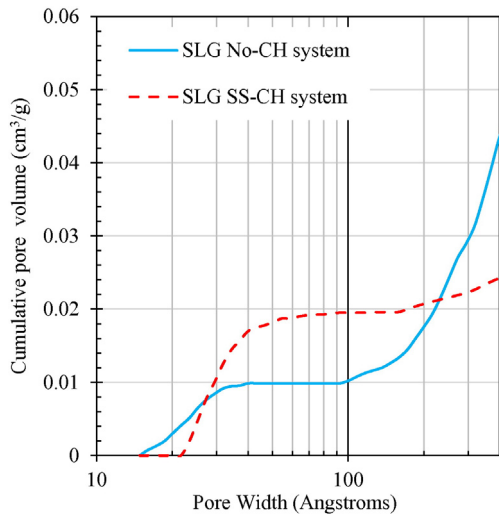


Fig. 14. Pore size distribution of corrosion products (1 week, 1 M NaOH, 60 °C). In reactor saturated with portlandite (SS-CH), corrosion products have lower porosity and smaller pore size.

Fig. 15 is a low magnification TEM image, showing the glass substrate and ordered corrosion products in the SS-CH reactor. High resolution TEM imaging (Fig. 16) showed a seemingly continuous transition between the glass substrate to the corrosion products, with randomly dispersed crystal nuclei (Fig. 16a). There was not a systematic trend for appearance of these crystals and in some cases, small crystalline nuclei were even observed within the glass substrate. By moving within the corrosion products layer away from the glass interface and towards the solution, the number and size of crystals increased considerably (Fig. 16b).

5. Discussion

Congruent dissolution of soda-lime glass in 1 M NaOH solution and in the absence of added $\text{Ca}(\text{OH})_2$ was observed to progress linearly with time at temperatures 20 to 80 °C. This agrees with dissolution regime II (constant rate) introduced by Frugier et al. [18]. It resulted in formation of two overlying corrosion products layers; an ordered layer resulting from in-situ alteration of glass, underneath a disordered

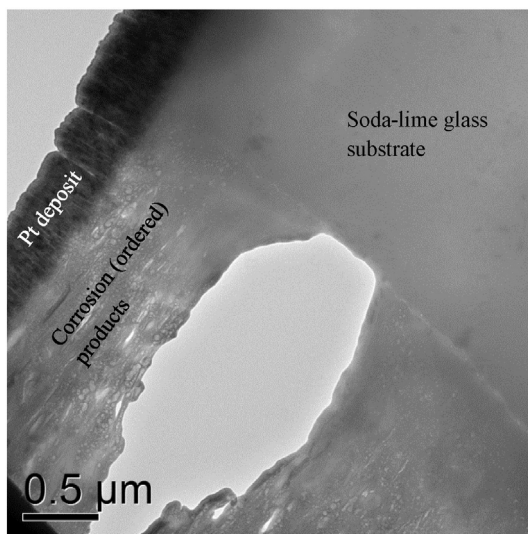


Fig. 15. TEM image of the thin section of soda-lime SS-CH glass showing corrosion products on the surface of glass slide (the hole in the center is a damaged area during the FIB process).

layer precipitated from the solution. Both layers contained crystalline C-S-H, whose formation is likely facilitated by the elevated temperature of the experiment (60 °C). The C-S-H had a fairly low Ca/Si (= 0.54 to 0.78 molar ratio), considerable Na/Si, and a high porosity, resulting in a weak bond to the substrate glass. Due to their high porosity, the corrosion products layers in this system did not cause a measurable drop in the glass dissolution rate.

In this system (soda-lime No-CH with low SA/V), Ca and Si was provided entirely by the glass (Ca/Si = 0.09). Initially, the congruent dissolution of glass released both Ca and Si into the solution (Fig. 9b). However, at approximately 3 to 4 days, all of the dissolved Ca precipitated back on the glass surface as C-S-H. Beyond this time, further glass dissolution/alteration only released Si into the solution while Ca was locally bound, possibly by the ordered corrosion products. Due to the absence of Ca in the solution (Ca/Si = 0.003), no ASR gel formed and dissolved Si remains in the solution. However, had glass dissolution occurred within a confined space (e.g., inside an intra-particle crack in Fig. 3a or in a high SA/V system), the combination of high concentration of dissolved Si and local availability of Ca at glass surface could form deleterious ASR gel.

In the SS-CH reactor, where the solution was maintained saturated with $\text{Ca}(\text{OH})_2$, the available aqueous Ca reacted with dissolved silica to form a denser, stronger, lower porosity, higher Ca/Si (= 1.28 molar ratio), and negligible Na/Si (= 0.06 molar ratio) C-S-H layer on the surface of glass. This is essentially an inner product pozzolanic C-S-H, which was formed by in-situ transformation of glass as opposed to precipitation from the solution, and as such, does not contain capillary pores (the majority of its pores are <10 nm). The solution remained practically free of dissolved Si and saturated with $\text{Ca}(\text{OH})_2$. The dissolution of glass was significantly reduced but not stopped (in agreement with regime IV (residual rate) of Frugier et al. [18]). This is most likely attributed to the protective nature of the C-S-H layer, providing a diffuse barrier against penetration of OH^- and Na^+ ions. This is why the outside surface of soda-lime glass particles is protected in portland cement systems (Fig. 3a to c), where the pore solution is locally saturated with $\text{Ca}(\text{OH})_2$, but is not protected in binders that do not form $\text{Ca}(\text{OH})_2$ (Fig. 3d).

As a final comment, we should acknowledge that the barrier nature of the C-S-H layer is a delicate balance. Since the C-S-H layer is not fully impermeable, inward diffusing of OH^- , Na^+ , and Ca^{2+} from solution towards glass occur simultaneously (note that charge balance must be maintained). Among these, Ca is the slowest ion [54] and is most likely to be picked up along the way to replace a bound Na in a low Ca/Si C-S-H (this is termed alkali recycling [66]). As OH^- reaches and corrodes the glass surface, Ca availability is critical to determine the nature and deleteriousness of the corrosion products. If sufficient Ca is available, stable and innocuous C-S-H could be formed; but at low Ca concentrations, deleterious ASR gel forms. Since Ca penetrates slower than Na and OH, it is possible that in some systems, ASR gel forms underneath an outer C-S-H layer [58]. This C-S-H layer especially mitigates the outward diffusion of dissolved silica and as such, acts as a semi-permeable membrane [19].

6. Conclusions

- The dissolution rate of soda-lime (SL) glass in NaOH solutions increases with pH and is related to $[\text{OH}^-]^{0.2}$ up to pH = 14. However, higher pH results in slower dissolution. Several hypotheses were offered to explain why silica dissolution slows down at very high pH.
- The dissolution rate of SL glass is temperature dependent, and the activation energy of dissolution in 1 M NaOH was measured as $87.5 \text{ kJ} \cdot \text{mol}^{-1}$.
- Presence of Ca ions in solution has a remarkable impact on reducing the dissolution rate of SL glass at high pH. This is likely due to formation of a dense, low porosity, high Ca/Si, and strongly bonded C-S-H layer on the surface of glass, which provides a diffuse barrier against

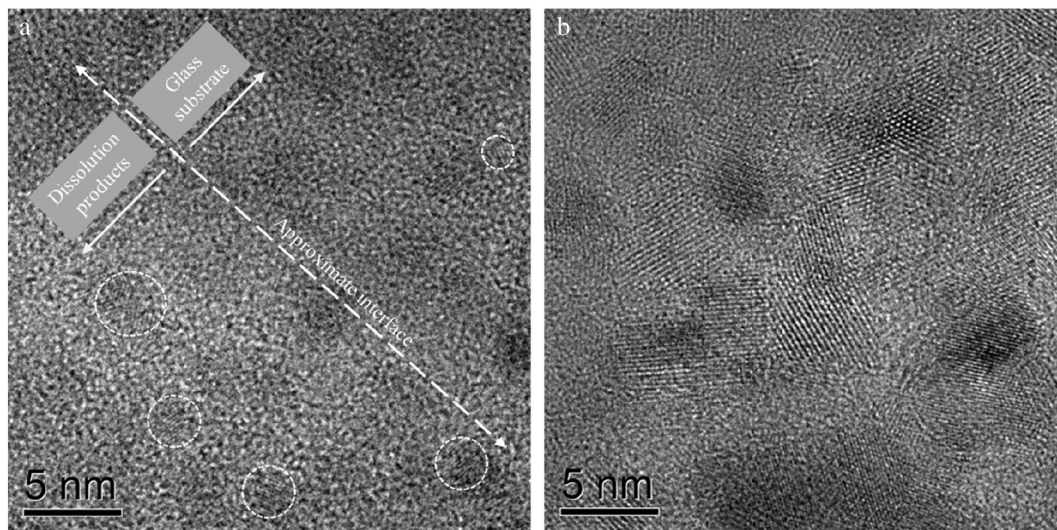


Fig. 16. TEM image of (a) the interface of substrate soda-lime glass and corrosion products, showing nucleation of crystals, (b) several crystals further away from the interface.

penetration and attack of OH^- and alkali ions. This is an inner product pozzolanic C–S–H, and is formed by in-situ transformation of glass as opposed to precipitation from the solution; and as such, does not contain capillary pores (the majority of its pores are <10 nm).

- In the absolute absence of Ca, the dissolved silica remains in the solution. However, if there is some, but insufficient, Ca available in the solution, it is consumed in reaction with the dissolving silica and forms low Ca/Si alkali-bearing C–S–H products that are loosely bonded to the surface of silica glass. Due to their porosity, these products cannot protect the glass substrate from further dissolution.
- The findings can explain why in portland cement concrete, soda-lime glass aggregates undergo ASR within their intra-particle cracks but not at the glass-cement paste interface.

Acknowledgements

The authors gratefully acknowledge support received from the National Science Foundation (NSF) under Grant No. 1030708 and the CAREER Award No. 1254333, granted to the second author. Any opinions, findings and conclusions or recommendations expressed in this material are those of the authors and do not necessarily reflect the views of the National Science Foundation.

References

- [1] H. Maraghechi, M. Maraghechi, F. Rajabipour, C. Pantano, Pozzolanic reactivity of recycled glass powder at elevated temperatures: reaction stoichiometry, reaction products, and effect of alkali activation, *Cem. Concr. Compos.* 53 (2014) 105–114.
- [2] C.A. Utton, R.J. Hand, P.A. Bingham, N.C. Hyatt, S.W. Swanton, S.J. Williams, Dissolution of vitrified wastes in a high-pH calcium-rich solution, *J. Nucl. Mater.* 435 (1–3) (2013) 112–122.
- [3] X. Hou, L.J. Struble, R.J. Kirkpatrick, Formation of ASR gel and the roles of C–S–H and portlandite, *Cem. Concr. Res.* 34 (2004) 1683–1696.
- [4] M.D.A. Thomas, The Role of Calcium in Alkali-Silica Reaction, *Materials Science of Concrete* (Sidney Diamond Symposium), The American Ceramic Society, Ohio, USA 1998, pp. 325–337.
- [5] F. Rajabipour, E. Giannini, C. Dunant, J.H. Ideker, M.D.A. Thomas, Alkali-silica reaction: current understanding of the reaction mechanisms and the knowledge gaps, *Cem. Concr. Res.* 76 (2015) 130–146.
- [6] A.K. Varshneya, *Fundamentals of Inorganic Glasses*, second ed. Academic Press Inc, San Diego, CA, 1994.
- [7] F. Gaboriaud, D. Chaumont, A. Nonat, B. Hanquet, A. Craevich, Study of the influence of alkaline ions (Li, Na and K) on the structure of the silicate entities in silico alkaline sol and on the formation of the silico-calco-alkaline gel, *J. Sol-Gel Sci. Technol.* 13 (1–3) (1998) 353–358.
- [8] B.C. Bunker, Molecular mechanism for corrosion of silica and silicate glasses, *J. Non-Cryst. Solids* 179 (1994) 300–308.
- [9] R.W. Douglas, T.M. El-Shamy, Reactions of glasses with aqueous solutions, *J. Am. Ceram. Soc.* 50 (1) (1967) 1–7.
- [10] R. Snellings, Surface chemistry of calcium aluminosilicate glasses, *J. Am. Ceram. Soc.* 98 (1) (2015) 303–314.
- [11] D.E. Clark, M.F. Dilmore, E.C. Ethridge, L.L. Hench, Aqueous corrosion of soda-silica and soda-lime-silica glass, *J. Am. Ceram. Soc.* 59 (1976) 62–65.
- [12] C.G. Pantano, A.E. Clark, L.L. Hench, Multilayer corrosion films on bioglass surfaces, *J. Am. Ceram. Soc.* 57 (9) (1974) 412–413.
- [13] S.C. Kohn, R. Dupree, M.E. Smith, Proton environments and hydrogen-bonding in hydrous silicate glasses from proton NMR, *Nature* 337 (1989) 539–541.
- [14] D.E. Clark, B.K. Zaitos, *Corrosion of Glass, Ceramics, and Ceramic Superconductors: Principles, Testing, Characterization, and Applications*, Chapter 5, Noyes Publication, USA, 1992.
- [15] H. Scholze, Chemical durability of glasses, *J. Non-Cryst. Solids* 52 (1–3) (1982) 91–103.
- [16] H. Scholze, Glass–water interactions, section 1. Water and glass, durability, and transport phenomena, *J. Non-Cryst. Solids* 102 (1988) 1–10.
- [17] A. Paul, *Chemistry of Glasses*, second ed. Chapman and Hall, New York, NY, 1990.
- [18] P. Frugier, S. Gin, Y. Minet, T. Chave, B. Bonin, N. Godon, J.E. Lartigue, P. Jollivet, A. Ayrat, L. De Windt, G. Santarini, SON68 nuclear glass dissolution kinetics: current state of knowledge and basis of the new GRAAL model, *J. Nucl. Mater.* 380 (2008) 8–21.
- [19] T.C. Powers, H.H. Steinour, An interpretation of some published researches on the alkali-aggregate reaction part 1—the chemical reactions and mechanism of expansion, *J. Am. Concr. Inst.* 51 (2) (1955) 497–516.
- [20] R.D. Aines, H.C. Weed, J.K. Bates, Hydrogen Speciation in Hydrated Layers on Nuclear Waste Glass, *Mat Res Soc Symp* 1987, pp. 547–558.
- [21] J.V. Walther, H.C. Helgeson, Calculation of the thermodynamic properties of aqueous silica and the solubility of quartz and its polymorphs at high pressures and temperatures, *Am. J. Sci.* 277 (1977) 1315–1351.
- [22] R.K. Iler, *The Chemistry of Silica: Solubility, Polymerization, Colloid and Surface Properties, and Biochemistry*, John Wiley and Sons, Inc., New York, 1979.
- [23] S. Sjöberg, Silica in aqueous environments, *J. Non-Cryst. Solids* 196 (1996) 51–57.
- [24] F. Gaboriaud, A. Nonat, D. Chaumont, Aggregation and gel formation in basic silico-calco-alkaline solutions studied: a SAXS SANS, and ELS study, *J. Phys. Chem. B* 103 (28) (1999) 5775–5781.
- [25] I.L. Svensson, S. Sjöberg, L. Ohman, Polysilicate equilibria in concentrated sodium silicate solutions, *J. Chem. Soc. Faraday Trans. 1* (82) (1986) (3655–3646).
- [26] O. Weres, A. Yee, L. Tsao, Kinetics of silica polymerization, *J. Colloid Interface Sci.* 84 (2) (1981) 379–402.
- [27] L. Nicoleau, A. Nonat, D. Perrey, The di- and tricalcium silicate dissolutions, *Cem. Concr. Res.* 47 (2013) 14–30.
- [28] P. Juilland, E. Gallucci, Morpho-topological investigation of the mechanisms and kinetic regimes of alite dissolution, *Cem. Concr. Res.* 76 (2015) 180–191.
- [29] S. Liu, K. Ferrand, K. Lemmens, Transport- and surface reaction-controlled SON68 glass dissolution at 30 °C and 70 °C and pH = 13.7, *Appl. Geochem.* 61 (2015) 302–311.
- [30] T.A. Abrajano, J.K. Bates, A.B. Woodland, J.P. Bradley, W.L. Bourcier, Secondary phase formation during nuclear waste glass dissolution, *Clay Clay Miner.* 38 (5) (1990) 537–548.
- [31] T. Chave, P. Frugier, S. Gin, A. Ayrat, Glass–water interphase reactivity with calcium rich solutions, *Geochim. Cosmochim. Acta* 75 (15) (2011) 4125–4139.
- [32] S. Mercado-Depierre, F. Angeli, F. Frizon, S. Gin, Antagonist effects of calcium on borosilicate glass alteration, *J. Nucl. Mater.* 441 (1) (2013) 402–410.
- [33] M. Fournier, S. Gin, P. Frugier, Resumption of nuclear glass alteration: state of the art, *J. Nucl. Mater.* 448 (2014) 348–363.
- [34] R. Snellings, Solution-controlled dissolution of supplementary cementitious materials at pH 13: the effect of solution composition on glass dissolution rates, *J. Am. Ceram. Soc.* 96 (8) (2013) 2467–2475.

- [35] C.A. Utton, R.J. Hand, N.C. Hyatt, S.W. Swanton, S.J. Williams, Formation of alteration products during dissolution of vitrified ILW in a high-pH calcium-rich solution, *J. Nucl. Mater.* 442 (1) (2013) 33–45.
- [36] Y. Oka, M. Tomozawa, Effect of alkaline earth ion as an inhibitor to alkaline attack on silica glass, *J. Non-Cryst. Solids* 42 (1–3) (1980) 535–543.
- [37] Y. Oka, K.S. Ricker, M. Tomozawa, Calcium deposition on glass surface as an inhibitor to alkaline attack, *J. Am. Ceram. Soc.* 62 (11–12) (1979) 631–632.
- [38] L. Armelao, A. Bassan, R. Bertoncello, G. Biscontin, S. Daolio, A. Glisent, Silica glass interaction with calcium hydroxide: a surface chemistry approach, *J. Cult. Herit.* 1 (4) (2000) 375–384.
- [39] N. Rajmohan, P. Frugier, S. Gin, Composition effects on synthetic glass alteration mechanisms: part 1. Experiments, *Chem. Geol.* 279 (2010) 106–119.
- [40] S. Gin, X. Beaudoux, F. Angéli, C. Jégou, N. Godon, Effect of composition on the short-term and long-term dissolution rates of ten borosilicate glasses of increasing complexity from 3 to 30 oxides, *J. Non-Cryst. Solids* 358 (18–19) (2012) 2559–2570.
- [41] A. Shayan, A. Xu, Value-added utilisation of waste glass in concrete, *Cem. Concr. Res.* 34 (1) (2004) 81–89.
- [42] C. Shi, Y. Wu, C. Reifler, H. Wang, Characteristics and pozzolanic reactivity of glass powders, *Cem. Concr. Res.* 35 (5) (2005) 987–993.
- [43] N. Schwarz, N. Neithalath, Influence of a fine glass powder on cement hydration: comparison to fly ash and modeling the degree of hydration, *Cem. Concr. Res.* 38 (2008) 429–436.
- [44] L.M. Federico, S.E. Chidiac, Waste glass as a supplementary cementitious material in concrete – critical review of treatment methods, *Cem. Concr. Compos.* 31 (4) (2009) 606–610.
- [45] K. Afshinnia, P.R. Rangaraju, Influence of fineness of ground recycled glass on mitigation of alkali–silica reaction in mortars, *Constr. Build. Mater.* 81 (2015) 257–267.
- [46] C. Polley, S.M. Cramer, R.V. De La Cruz, Potential for using waste glass in Portland cement concrete, *J. Mater. Civ. Eng.* 10 (4) (1998) 210–219.
- [47] W. Jin, C. Meyer, S. Baxter, Glascrete–concrete with glass aggregate, *ACI Mater. J.* 97 (2) (2000) 208–213.
- [48] J.R. Wright, C. Cartwright, D. Fura, F. Rajabipour, Fresh and hardened properties of concrete incorporating recycled glass as 100% sand replacement, *ASCE J. Mater. Civ. Eng.* 26 (10) (2014).
- [49] F. Rajabipour, H. Maraghechi, G. Fischer, Investigating the alkali silica reaction of recycled glass aggregates in concrete materials, *J. Mater. Civ. Eng.* 22 (12) (2010) 1201–1210.
- [50] F. Rajabipour, H. Maraghechi, S.M.H. Shafaatian, ASR and its Mitigation in Mortars Containing Recycled Soda-Lime Glass Aggregates, 14th International Conference on Concrete Alkali Aggregate Reactions (ICAAAR), Austin, Texas, 2012.
- [51] H. Maraghechi, S.M.H. Shafaatian, G. Fischer, F. Rajabipour, The role of residual cracks on alkali silica reactivity of recycled glass aggregates, *Cem. Concr. Compos.* 34 (2012) 41–47.
- [52] M.S. Tarnopol, A.E. Junge, Resistance of plate glass to alkaline solutions, *J. Am. Ceram. Soc.* 29 (2) (1946) 36–39.
- [53] L.A. Bromley, Thermodynamic properties of strong electrolytes in aqueous solutions, *AICHE J.* 19 (2) (1973) 313–320.
- [54] CRC Handbook of Chemistry and Physics, 90th ed. CRC Press, Boca Raton, Florida, 2010.
- [55] W.H. Casey, G. Sposito, On the temperature dependence of mineral dissolution rates, *Geochim. Cosmochim. Acta* 56 (10) (1992) 3825–3830.
- [56] I.G. Richardson, The calcium silicate hydrates, *Cem. Concr. Res.* 38 (2) (2008) 137–158.
- [57] H.F.W. Taylor, *Cement Chemistry*, Academic Press, San Diego, California, USA, 1990.
- [58] R.F. Bleszynski, M.D.A. Thomas, Microstructural studies of alkali–silica reaction in fly ash concrete immersed in alkaline solutions, *Adv. Cem. Based Mater.* 7 (2) (1998) 66–78.
- [59] A. Gholizadeh Vayghan, F. Rajabipour, J.L. Rosenberger, Composition–rheology relationships in alkali–silica reaction gels and the impact on the gels' deleterious behavior, *Cem. Concr. Res.* 83 (2016) 45–56.
- [60] A. Gholizadeh Vayghan, F. Rajabipour, C. Arndt, The Influence of ASR Gels Composition on their Swelling Properties, 15th International Conference on Concrete Alkali Aggregate Reactions (ICAAAR), Sao Paulo, Brazil, 2016.
- [61] G. Constantinides, F.-J. Ulm, The effect of two types of C–S–H on the elasticity of cement-based materials: results from nanoindentation and micromechanical modeling, *Cem. Concr. Res.* 34 (1) (2004) 67–80.
- [62] E. Bonaccorsi, S. Merlino, A.R. Kampf, The crystal structure of tobermorite 14 (plombierite), a C–S–H phase, *J. Am. Ceram. Soc.* 88 (3) (2005) 505–512.
- [63] F. Battocchio, P.J.M. Monteiro, H. Wenk, Rietveld refinement of the structures of 1.0 C–S–H and 1.5 C–S–H, *Cem. Concr. Res.* 42 (11) (2012) 1534–1548.
- [64] M.C.G. Juenger, H.M. Jennings, The use of nitrogen adsorption to assess the microstructure of cement paste, *Cem. Concr. Res.* 31(6) 883–892
- [65] K.K. Aligizaki, *Pore Structure of Cement-Based Materials*, Taylor and Francis, London, 2006.
- [66] M.D.A. Thomas, The role of calcium hydroxide in alkali recycling in concrete, calcium hydroxide in concrete, *Mater. Sci. Concr.* (2001) 225–236 (special issue).